Computerized Medical Imaging and Graphics 33 (2009) 256–266

Contents lists available at ScienceDirect

Computerized Medical Imaging and Graphics

journal homepage: www.elsevier.com/locate/compmedimag

Acquisition-related motion compensation for digital subtraction angiography

Razvan Ioan Ionasec [a,c], Benno Heigl [b], Joachim Hornegger [c,d,*]

[a] Siemens Corporate Research, Princeton, NJ, USA
[b] Siemens AG, Med, PLM-E IC, Forchheim, Germany
[c] Department of Computer Science, Chair of Pattern Recognition, Friedrich-Alexander Uninversity, Erlangen-Nurmenberg, Germany
[d] Erlangen Graduate School in Advanced Optical Technologies (SAOT), Erlangen, Germany

ARTICLE INFO

Article history:
Received 23 January 2007
Received in revised form 4 October 2008
Accepted 15 December 2008

Keywords:
Digital subtraction angiography
Motion compensation
3D rigid registration
Interventional angiography
Road mapping

ABSTRACT

Subtraction methods in angiography are generally applied in order to enhance the visualization of blood vessels by eliminating bones and surrounding tissues from X-ray images. The main limitation of these methods is the sensitivity to patient movement, which leads to artifacts and reduces the clinical value of the subtraction images. In this paper we present a novel method for rigid motion compensation with primary application to road mapping, frequently used in image-guided interventions. Using the general concept of image-based registration, we optimize the physical position and orientation of the C-arm X-ray device, thought of as the rigid 3D transformation accounting for the patient movement. The registration is carried out using a hierarchical optimization strategy and a similarity measure based on the variance of intensity differences, which has been shown to be most suitable for fluoroscopic images. Performance evaluation demonstrated the capabilities of the proposed approach to compensate for potential intra-operative patient motion, being more resilient to the fundamental problems of pure image-based registration.

1. Introduction

Digital subtraction angiography (DSA) is a powerful technique for the visualization of blood vessels in the human body comprising various applications in medicine. Since blood has almost the same radio-density as the surrounding tissues, vessels become visible in X-ray images by filling them with a contrast agent. Furthermore, the image quality can be considerably enhanced through the subtraction of a native image acquired without contrast agent from a second image of the vessels that have been filled with contrast agent. In the resulting image, bones and surrounding tissues are ideally masked out after subtraction, enabling an optimal evaluation of blood vessels (see Fig. 1(a)).

Besides diagnostic usability, DSA became more important in image-guided interventions. Combined with real-time fluoroscopy, it is applied to facilitate various minimally invasive interventional procedures. These include percutaneous transluminal angioplasty (PTA), repair of vascular stenoses aneurysms via stenting and coiling, placement of tranjugular intrahepatic portosystemic shunts (TIPS), biopsies, and pain therapy [1]. An important imaging technique, referred to as road mapping (RM), is used to guide the advancement of catheters and other devices during minimally invasive interventions. Continuously acquired native images are subtracted from a previously acquired fill image (mask), commonly showing a black catheter advancing through white vessels [2](see Fig. 2(a)).

Regardless of the application, DSA is based on the assumption that structures surrounding the vessels do not change their position during acquisition. This was shown to be the main limitation for DSA since this assumption is not valid in a substantial number of cases due to patient movement during clinical procedures [3–5]. The introduced motion artifacts reduce the quality of the subtraction images and affect their clinical interpretation (see Figs. 1b and 2b). Consequently, the image acquisition process has to be repeated for a significant number of cases, which represents a drastic disadvantage especially in time critical image-guided interventions. Furthermore, patients have to cope with additional stress through contrast agent and radiation exposure.

Since 1980 various approaches have been proposed for the reduction of motion artifacts in DSA (see Section 2). Their clinical applicability, however, is limited due to various characteristic restrictions. Patient and acquisition-related solutions, such as immobilization [6] or ECG gating [7], account only for specific motion, while image-based methods [8,9] are not robust against relatively large misalignments.

* Corresponding author at: Department of Computer Science, Chair of Pattern Recognition, Friedrich-Alexander Uninversity Erlangen-Nurmenberg, Germany. Tel.: +49 9131 85 27883; fax: +49 9131 303811.
E-mail addresses: Razvan_Ionasec.ext@siemens.com (R.I. Ionasec), Benno.Heigl@siemens.com (B. Heigl), Joachim.Hornegger@informatik.uni-erlangen.de (J. Hornegger).

0895-6111/$ – see front matter © 2008 Elsevier Ltd. All rights reserved.
doi:10.1016/j.compmedimag.2008.12.006

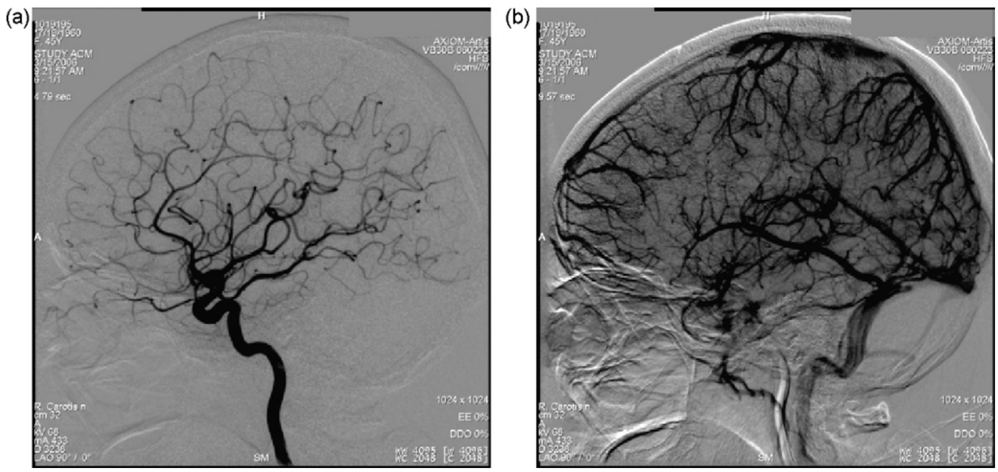

Fig. 1. Example of DSA diagnoses. (a) Head vasculature visualization through digital subtraction angiography and (b) artifacts caused by patient motion.

In this paper we present a novel approach for motion artifact compensation, primarily designed for RM. Our method combines the advantages of acquisition-related solutions with image-based registration into a motion-compensation framework more resilient to the fundamental problems of pure image processing techniques. The misalignment between the native and fill image can be corrected before the digital subtraction if the parameters of the disturbing motion are known. Assuming the patient movement in the 3D space is rigid, it can be described by a geometrical transformation with six parameters (translation and rotation). Within our approach, this rigid 3D transformation is represented by the physical position parameters of a C-arm X-ray acquisition system with six degrees of freedom.

Instead of transforming the native image to match the mask image, as in classical image-based registration, the position of the C-arm X-ray system for which the disturbing motion is compensated is estimated. Consequently, a new native image acquired from the estimated position of the C-arm X-ray system is, in the ideal case, perfectly aligned with the mask image. The estimation process is performed iteratively through a hierarchical optimization strategy, and requires multiple acquisitions of X-ray images from different positions. Image-based methods can be independently applied posterior to the proposed motion-compensation approach to correct potential non-rigid misalignments.

Our main contributions are as follows:

- The formulation of the artifact correction in DSA as a motion-compensation problem, which is solved by optimizing the physical position of the C-arm acquisition system.
- The performance evaluation of six classic intensity-based similarity measures on fluoroscopic images acquired under intervention circumstances.
- The design and implementation of an efficient hierarchical optimization algorithm for acquisition-based registration approaches of DSA images.

In the following, the organization of this paper is presented. Section 2 provides a brief overview on existing artifact correction methods proposed in the literature. In Section 3 the novel approach for motion compensation in DSA is described in more detail. Experimental results are presented and interpreted in Section 4. Finally, in Section 5 presents perspectives for future work and overall conclusions.

2. Related work

In most cases, motion artifacts significantly reduce the clinical relevance of DSA images. Various solutions for this problem were proposed over the past two decades.

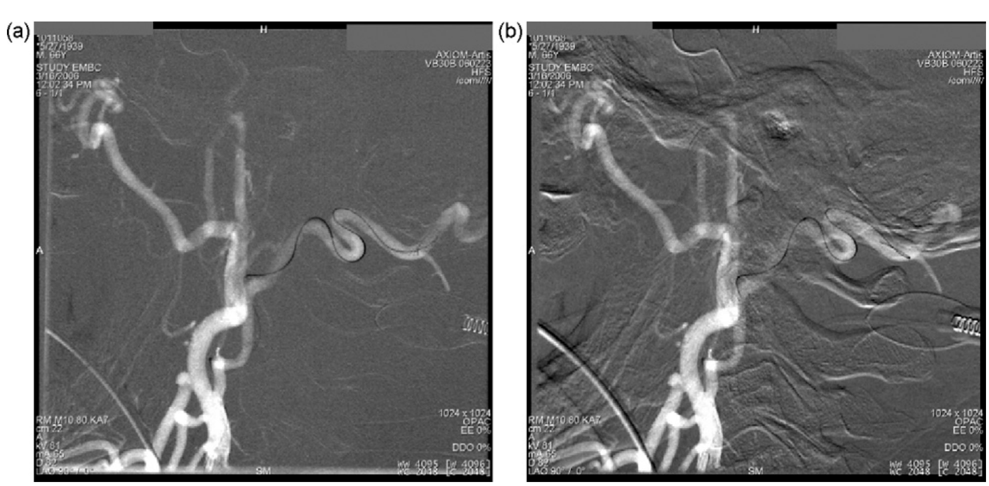

Fig. 2. Example of road mapping (RM). (a) Catheter guidance supported through RM and (b) artifacts caused by patient motion.

2.1. Patient and acquisition-related solutions

Straightforward techniques, focused on avoiding patient movement during exposure, have been proposed and applied in some cases including arms, legs and head immobilization techniques [6]. Although these methods reduce motion artifacts in various diagnostical procedures, they are not applicable in long-lasting interventional procedures.

Motion artifacts caused by the pulsation of vascular structures can be avoided by using images acquired during the same cardiac phase [7]. Therefore, the QRS-complex in the ECG-curve is used to trigger the X-ray exposure. This technique requires special equipment and its not extendable for other movement sources.

Further, motion artifacts can be reduced by automatic re-masking during acquisition. Oung and Smith [10] used a real-time motion detector, based on the variance of the histogram of gray values in successive subtraction images, which can be considered as a measure of similarity between mask and fill image. A new mask image was acquired as soon as the measure exceeded a predefined threshold. This method enables artifact correction only if motion occurs before the contrast agent arrives at the vessels of interest.

These solutions have not become widely accepted in clinical environments, mainly because of their limited applicability or requirement for special materials and equipments, or both.

2.2. Image processing solution

Image registration techniques are more likely to be used in clinical practice since satisfying results can be achieved at low computational and material costs. These approaches perform a spatial transformation of one image relative to another in order to compute an optimal alignment, with respect to a given criterion.

The simplest, but also most popular registration method used in DSA is pixel shifting. According to this technique, the correspondence between the mask and the contrast image is achieved by manually shifting one image relatively to the other one. Despite existing semi-automatic versions, this remains a very rudimentary method especially due to the time-consuming and user-dependent operation.

In order to obtain more accurate motion correction, registration techniques have been designed to allow more local control. Meijering et al. [8] proposed a Block-Matching based non-rigid registration technique that yielded satisfactory results in DSA registration tasks. This process involves an edge-based selection of control points in the mask image for which the displacement is computed, taking a small block of certain amounts of pixels around each point and searching for the corresponding block in the contrast image. The two images are warped according to a displacement vector field constructed through interpolation. Bentoutou et al. [9] proposed a control point driven registration based on invariants similarity measure. After applying standard edge-detection approaches, control points are chosen based on the gradient magnitude and some neighborhood windowing. Point correspondence is achieved through sequentially performed template matching using invariant-based measures. The thin-plate-spline transformation is applied for the final warping between mask and contrast image.

Regardless of specific approaches, pure image-based registration methods are not completely solving the problems of motion artifacts, since these are suffering from three fundamental limitations [8]:

- **Overlapped region**—Only the overlapped region of two images can be optimally aligned through image-based registration (see Fig. 3(a)). The uncorrelated image regions remain misaligned presenting motion artifacts.
- **Superimposed structures**—Differences of two images can be caused by displacements of structures which are superimposed (see Fig. 3(b)). It is practically impossible to correct this type of appearance changes by deformations of the projection image.
- **Aperture problem**—The motion of a homogeneous contour is locally ambiguous due to the limited field of view of the X-ray detector. Subsequently, the component of the displacement vector for the tangential direction cannot be determined (see Fig. 3(c)).

3. Motion-compensation approach

The registration is formulated as a motion-compensation problem, which can be thought of as a classical pose estimation problem [11]. Instead of estimating a geometrical transformation, as in common image-based registration approaches, the pose of the acquisition system is determined, for which the disturbing motion artifacts are corrected.

We assume that patient motion do not cause flexible deformation in the area of interest and consequently can be estimated accurately enough using a rigid 3D transformation (1), which includes rotation and translation. This transformation is represented by the pose of a C-arm X-ray acquisition system with six degrees of freedom. The pose estimation is formulated as an optimization problem of an objective function defined by a similarity measure over a six dimensional discrete search space D.

$$T_{3D} = \begin{pmatrix} \cos\beta\cdot\cos\gamma & \cos\alpha\cdot\sin\gamma+\sin\alpha\cdot\sin\beta\cdot\cos\gamma & \sin\alpha\cdot\sin\gamma-\cos\alpha\cdot\sin\beta\cdot\cos\gamma & t_x \\ -\cos\beta\cdot\sin\gamma & \cos\alpha\cdot\cos\gamma-\sin\alpha\cdot\sin\beta\cdot\sin\gamma & \sin\alpha\cdot\cos\gamma-\cos\alpha\cdot\sin\beta\cdot\sin\gamma & t_y \\ \sin\beta & -\sin\alpha\cdot\cos\beta & \cos\alpha\cdot\cos\beta & t_z \\ 0 & 0 & 0 & 1 \end{pmatrix} \quad (1)$$

In order to increase efficiency and accuracy the discrete search space D has been pruned regarding the maximal practical patient motion during interventional procedures for each of the six dimensions. The considered intervals are $(-5, 5)^\circ$ for the rotation parameters and $(-3, 3)$ cm for the translation parameters, where the positioning precision of the C-arm X-ray acquisition system is 0.1°, respectively centimeters.

The proposed algorithm is demonstrated in Fig. 4. Initially, the fill (mask) image is acquired preprocessed and stored. Iteratively, native (live) images are acquired from different positions, and compared to the mask image using an intensity-based measure. The algorithm terminates when the global minimum of the measure is reached. Image-based registration methods can be applied afterwards for refining potential non-rigid misalignments. Independent of a specific approach, these are expected to perform significantly more accurate applied after the rigid motion was corrected.

3.1. Acquisition system

In order to be adequate for our framework, the X-ray acquisition system has to fulfill several requirements. Crucial are the six parameters of the rigid 3D transformation which have to be mapped to the degrees of freedom of the acquisition system. The automatic steerable C-arm angulations (left/right anterior oblique, caudal/cranial, and detector rotation) and table movements (longitudinal, transversely and height adjustment) are associated with the rotation

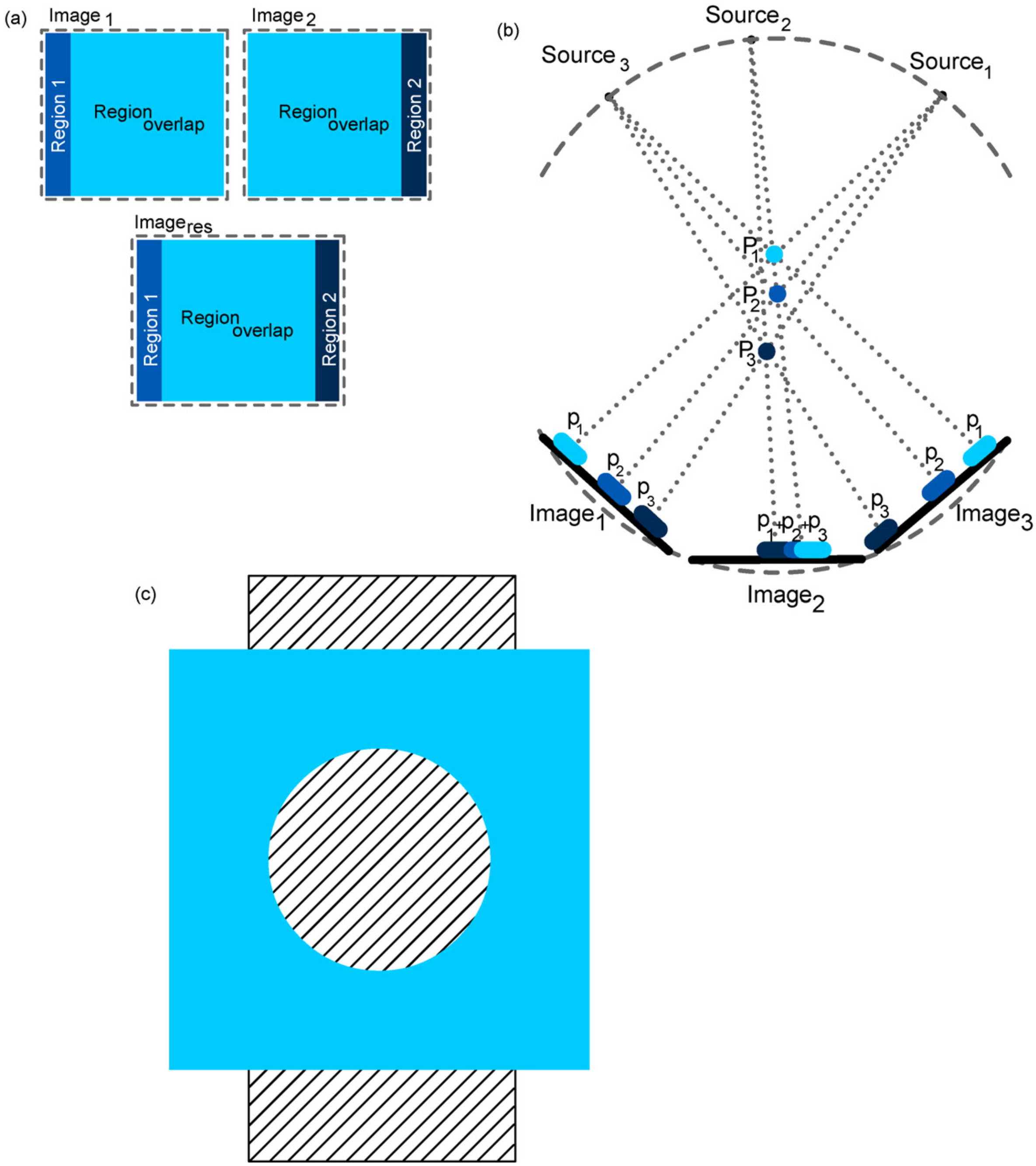

Fig. 3. (a) Image Image_{res} as result of the image-based registration of the images Image_1 and Image_2. Only the overlapped region $\text{Region}_{overlap}$ can be aligned correctly, since Region_1 and Region_2 remain misaligned. (b) The projections p_1, p_2, and p_3 of the points P_1, P_2, and P_3 for different positions of the X-ray source. It is important to mention that the same effects can be observed if the X-ray source remains fixed and the points are moving (due to patient motion). (c) If the stripes move upwards the pattern of lines in the aperture shifts. If the stripes move leftwards the pattern within the aperture shifts in the same way.

and translation parameters of the transformation. Moreover, fluoroscopy acquisition and DICOM compatibility should be granted in order to enable intra-operative application and online image transfer, respectively.

3.2. Similarity measure

The optimal solution is computed by minimizing an intensity-based similarity measure used to determine the amount of correspondence between the fill and the native image. Various similarity measures have been proposed in the literature for the registration of angiographic images [8,12–16], which however, were evaluated and applied to compare high-dose X-ray images used for diagnoses. In image-guided procedures, appearance changes of the acquired images are in general more complex depending on specific interventions and devices used. Furthermore, fluoroscopy (low-dose image acquisition) is more likely to be used in order to diminish the patient radiation exposure. With respect to these facts a suitable similarity measure for fluoroscopic images acquired during interventional procedures should be robust against the following factors of influence:

- Local gray level changes—caused not only by injected contrast medium but also by devices introduced during the intervention.

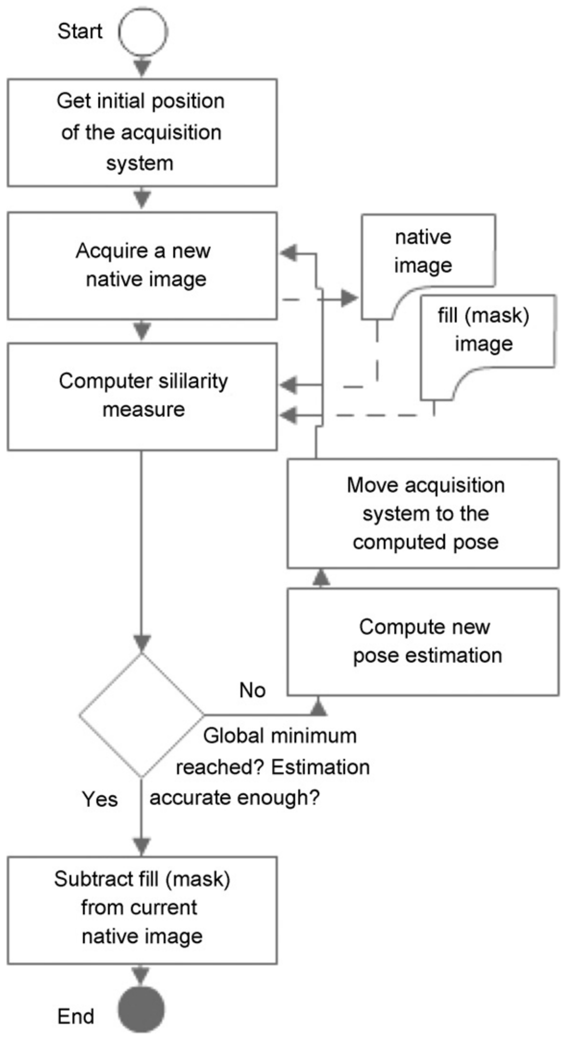

Fig. 4. Optimization process diagram.

- Quantum noise level—higher in fluoroscopy, since radiation dose is significantly lower compared to normal acquisition procedures.
- Additive mean gray-level offsets—caused by the exposure control of the X-ray acquisition system.

We extended the evaluation of intensity-based similarity measures to fluoroscopic road-map images and include the following distance methods:

- Sum of squared differences (SSD);
- Sum of absolute values of differences (SAVD);
- Ratio image uniformity (RIU);
- Normalized cross correlation (NCC);
- Variance of differences (VOD);
- Energy of histogram of differences (EHD).

A detailed presentation of the evaluation is given in Section 4.1. We conclude that the VOD (2) is the most adequate measure to determine the similarity between fluoroscopic images acquired during interventional procedures. Its global minimum is closer to the ground truth, being also more resilient to various noise sources.

$$d_{\mathrm{VOD}}(I_1, I_2(x_T)) = \frac{A-B}{N^2} \quad (2)$$

$$A = N \sum_{(i,j)\in W} (I_1(i,j) - I_2(x_T, i, j))^2 \quad (3)$$

$$B = \left(\sum_{(i,j)\in W} (I_1(i,j) - I_2(x_T, i, j)) \right)^2 \quad (4)$$

where W is used for a certain window (in our case the entire image), N represents the number of pixels in W, $I_*(i,j)$ denotes the intensity of an image I_* at coordinates (i,j), $I_*(x_T)$ stands for an (live) image acquired at position x_T. The vector x_T represents a position of the C-arm acquisition system expressed as $(\alpha, \beta, \gamma, t_x, t_y, t_z)$.

3.3. Optimization and validation

Within the optimization process, the position vector x_T^o defined over the six dimensional discrete search space D, is estimated, for which the VOD similarity measure assumes a global minimum (5).

$$x_T^o = \mathrm{argmin}_{x_T \in D} d_{\mathrm{VOD}}(I_1, I_2(x_T)) \quad (5)$$

where D is the discrete search space and $x_T \in D$.

The optimization has to be performed with a minimum of complexity since each additional iteration-step requires not only computation time and additional repositions of the acquisition device, but also increases the radiation exposure time of the patient. An exhaustive search of the optimum in the discrete space D requires appreciatively 10^9 iterations and it is obviously not applicable. Experimentally it was shown that global optimization strategies and gradient based methods are not suitable due to the large number of required iterations.

We propose a hierarchical optimization approach, which combines coarse and fine optimization algorithms as well as allows for estimation validation. The optimal parameter vector x_T^o, which is to be estimated, is initialized with a given start parameter vector x_T^s, which describes the current position of the acquisition system. The $e_1, e_2, \ldots e_6$ are the unit vectors and s_i^l, s_i^h are the low respectively high interval boundaries for each dimension i relative to x_t^s. As mentioned the feasible intervals are $(-3, 3)$ and $(-5, 5)$ for translation and, respectively, for the rotation. The function $f(x_T)$ stands for $d_{\mathrm{VOD}}(I_1, I_2(x_T))$.

(1) A coarse optimization phase is performed using the golden section search algorithm [17] adapted for a multidimensional search space. The following steps are carried out for each dimension i separately.
  (a) An initial bracketing interval (a, b, c) is selected with $a = s_i^l$, $b = 0$ and $c = s_i^h$.
  (b) If the condition $f(a \cdot e_i + x_T^o) > f(b \cdot e_i + x_T^o) < f(c \cdot e_i + x_T^o)$ is satisfied, the golden section search (step (c)) is performed. Otherwise, the current bracketing interval is recursively bisected until the above condition is satisfied. If the bracketing interval becomes smaller than Θ_b, the best parameter p, out of (a, b, c), is selected and x_T^o is replaced by $p \cdot e_i + x_T^o$. Since no valid bracketing interval could be found, the coarse optimization is finished for the current dimension i.
  (c) The golden section search is started with the computed valid bracketing interval (a, b, c). The algorithm terminates when the bracketing interval size is smaller than Θ_g, with an optimal parameter p ($p = b$ and $f(a \cdot e_i + x_T^o) > f(b \cdot e_i + x_T^o) < f(c \cdot e_i + x_T^o)$). x_T^o is replaced by the vector $p \cdot e_i + x_T^o$ and the coarse optimization is finished for the current dimension i.
  Parameters: Θ_b, Θ_g.
(2) The $N_p + 1 (N_p = 6)$ starting points needed by the downhill simplex algorithm [18] used in the fine optimization phase, are computed.

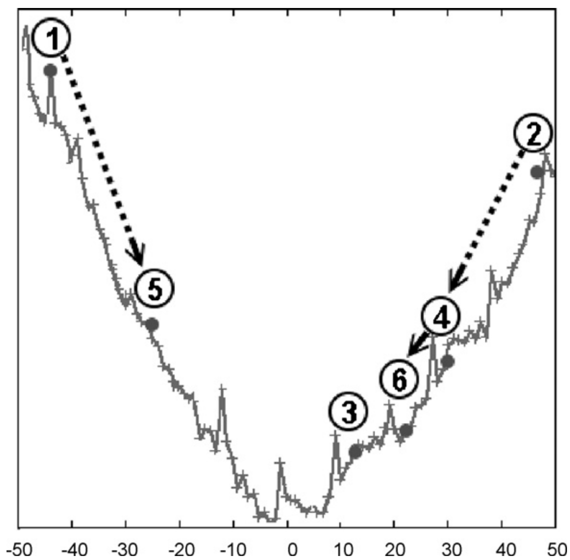

Fig. 5. The minimum is originally bracketed by points 1,3,2. The function is evaluated at 4, which replaces 2; then at 5, which replaces 1; then at 6, which replaces 4. The rule at each stage is to keep a center point that is lower than the two outside points. After the steps shown, the minimum is bracketed by points 5,3,6.

(a) The first point of the simplex P_0 is the optimal parameter vector x_T^o, computed by the coarse optimization. The other N_p points are mutations of x_T^o along each dimension separately.

(b) For each dimension i, $P_i = d \cdot e_i + x_T^o$. If the Euclidean distance between x_T^s and x_T^o, for the current dimension i is greater than Θ_s then $d = d_{\text{neg}}$, otherwise $d = d_{\text{pos}}$.

Parameters: Θ_s, d_{neg}, d_{pos}.

(3) The fine optimization is performed using the downhill simplex algorithm.

(a) The $N_p + 1$ starting points computed in step (2) are optimized by means of successive reflection and contraction of the simplex.

(b) If the Euclidean distance between the best and worst point of the simplex is smaller than Θ_d, the algorithm terminates and the optimal parameter vector x_T^o is replaced with the best simplex point.

Parameters: Θ_d.

(4) Validation of the optimum parameter vector x_T^o is performed.

(a) For each dimension i separately, the function f is evaluated at $v_l \cdot e_i + x_T^o$ and $v_h \cdot e_i + x_T^o$, and compared to $f(x_T^o)$.

(b) If $f(x_T^o)$ is still the minimum for each dimension, the optimization process will finish with the optimal parameter vector x_T^o. Otherwise, for each dimension i where the condition is not satisfied, x_T^o is replaced by $v_l \cdot e_i + x_T^o$ (if $f(v_l \cdot e_i + x_T^o) < f(v_h \cdot e_i + x_T^o)$) or by $v_h \cdot e_i + x_T^o$ (in the other case), and the steps 1–4 are repeated up to Θ_t times.

Parameters: Θ_t, v_l, v_h.

3.3.1. Coarse optimization

An approximation of the global minimum is achieved during the coarse optimization using a multi-dimensional extension of the golden section search algorithm [17]. Sequentially for each dimension, the interval bracketing the global minimum is reduced by 0.61803 each iteration. As the chosen sampling points are widespread over the search range, this method confers implicitly robustness against local minima (see Fig. 5). The parameters Θ_b and Θ_g of this optimization phase should be small enough in order to enable an acceptable approximation of the global extreme. However, if Θ_b and Θ_g are too small, unnecessary iterations are performed, wasting computation time. Based on experimental results we concluded that an accuracy of 10 units (1°, respectively 10 mm) is optimal.

3.3.2. Fine optimization

The coarse estimation is refined during the second optimization stage using the Nelder–Mead downhill simplex algorithm [18]. A $N + 1$simplex, generated from the initial estimation, abridges iteratively around the minimum following a set of predefined transformations (reflection, expansion, contraction, and multiple contraction). The parameters Θ_s, d_{neg} and d_{pos}, which determine the initial simplex, are chosen to maximize the probability of the nearest extremum to the simplex to be the global minimum. The Θ_d parameter describes the minimal allowed Euclidean distance between the best and worst point of the simplex and thus controlling the precision of the algorithm. Concerning the positioning precision of the acquisition system, Θ_d was set to 5 units.

3.3.3. Validation

A heuristic validation stage is introduced in order to increase the robustness of our algorithm by allowing avoidance of suboptimal solutions. The target function is evaluated for each dimension separately at two different points determined by the parameters v_l and v_h. The evaluated points should be far enough from the computed minimum in order to enable the optimization strategy to escape from a possible local extrema. Since locals observed during evaluation were not more distant than 10 units (1°, respectively 10 mm), a step of 15, respectively, −15 units should guarantee

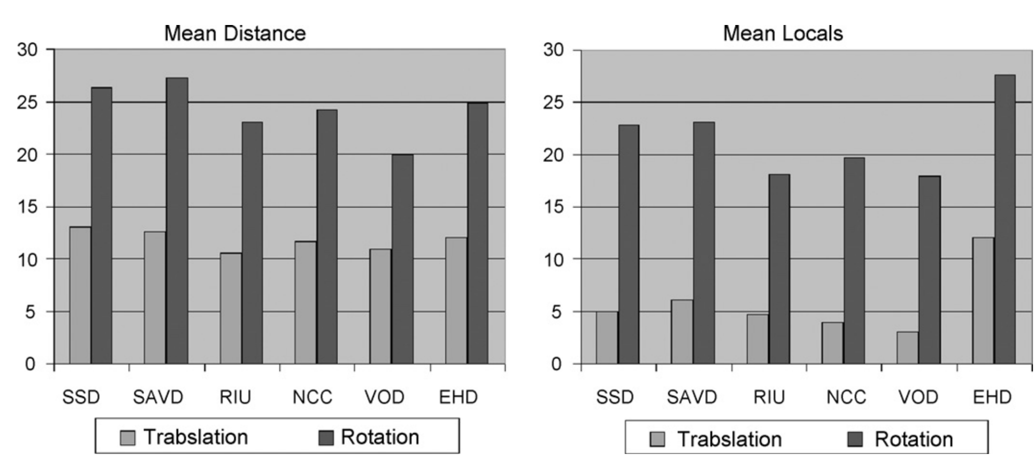

Fig. 6. (Left) The mean distance relative to the ground truth expressed in millimeters and 0.1° and (right) the mean number of local minima.

Table 1
Values of the parameters of the optimization algorithm used during the experiments described in the next chapter.

Parameter	Value
Θ_b	12
Θ_g	10
Θ_s	25
Θ_d	5
Θ_t	3
d_{neg}	−13
d_{pos}	13
v_l	−15
v_h	15

the robustness for this problem. The entire optimization process can be repeated up to Θ_t times, in case of validation failure. Θ_t is set 3 due to the maximal allowed low-dose exposure time of 6 min.

The parameters of the algorithm are given in Table 1 and were remained fixed during the experiments presented in Section 4.

4. Experimental results

The experiments were performed on the Siemens AXIOM Artis *d* MP C-arm X-ray acquisition system, which is a multi-purpose C-arm X-ray system with steerable angulations (rotations) and table position (translations). Image processing was carried out on a separate PC, not part of the AXIOM Artis *d* MP C-arm system, with the following configuration: Intel Pentium M 1100 MHz Processor, 512 MB RAM, Intel 855GME Graphic Chipset and Microsoft Windows XP Professional Edition operating system. The performance evaluation was performed on 4700 images acquired from head and abdomen phantoms manufactured out of real human bones. All images were acquired at a fluoroscopic energy level, with a resolution of 720 × 720 and pixel depth of 12 bits.

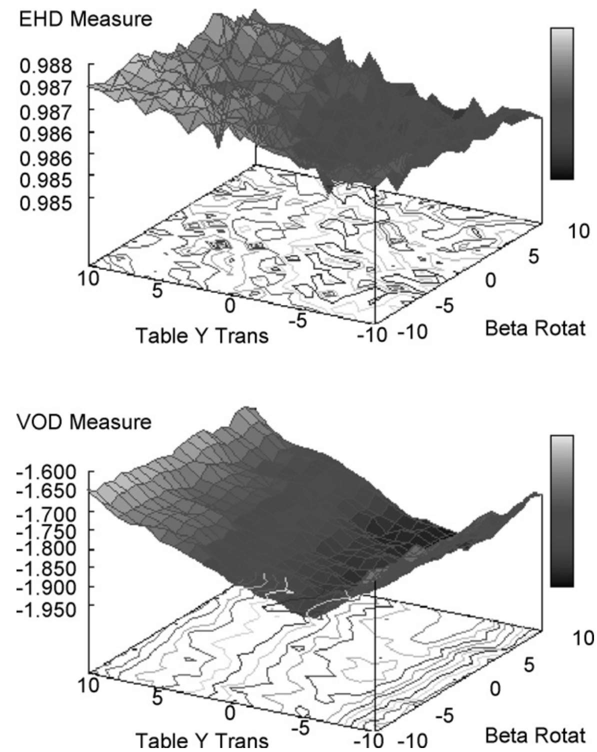

Fig. 8. EHD and VOD evaluation for the $t_y - \beta$ (Table Y Trans.–Beta Rotat.) dimensions and abdomen phantom.

4.1. Similarity measure

The evaluation of the similarity measures was performed on image series obtained by varying one or two position parameters while maintaining the others fixed. Such sequences were acquired

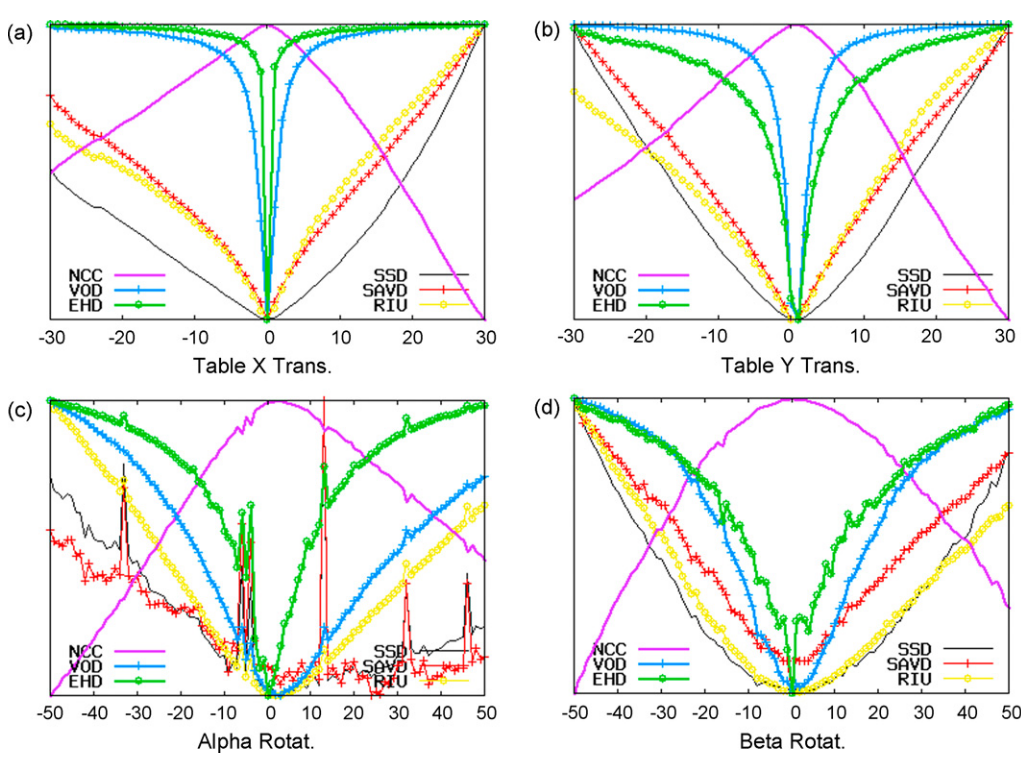

Fig. 7. Measures evaluation for different dimensions. (a) Evaluation of the t_x (Table X Trans.) dimension using the head phantom; (b) evaluation of the t_y (Table Y Trans.) dimension using the head phantom; (c) evaluation of the α (Alpha Rotat.) dimension using the abdomen phantom; (d) evaluation of the β (Beta Rotat.) dimension using the head phantom.

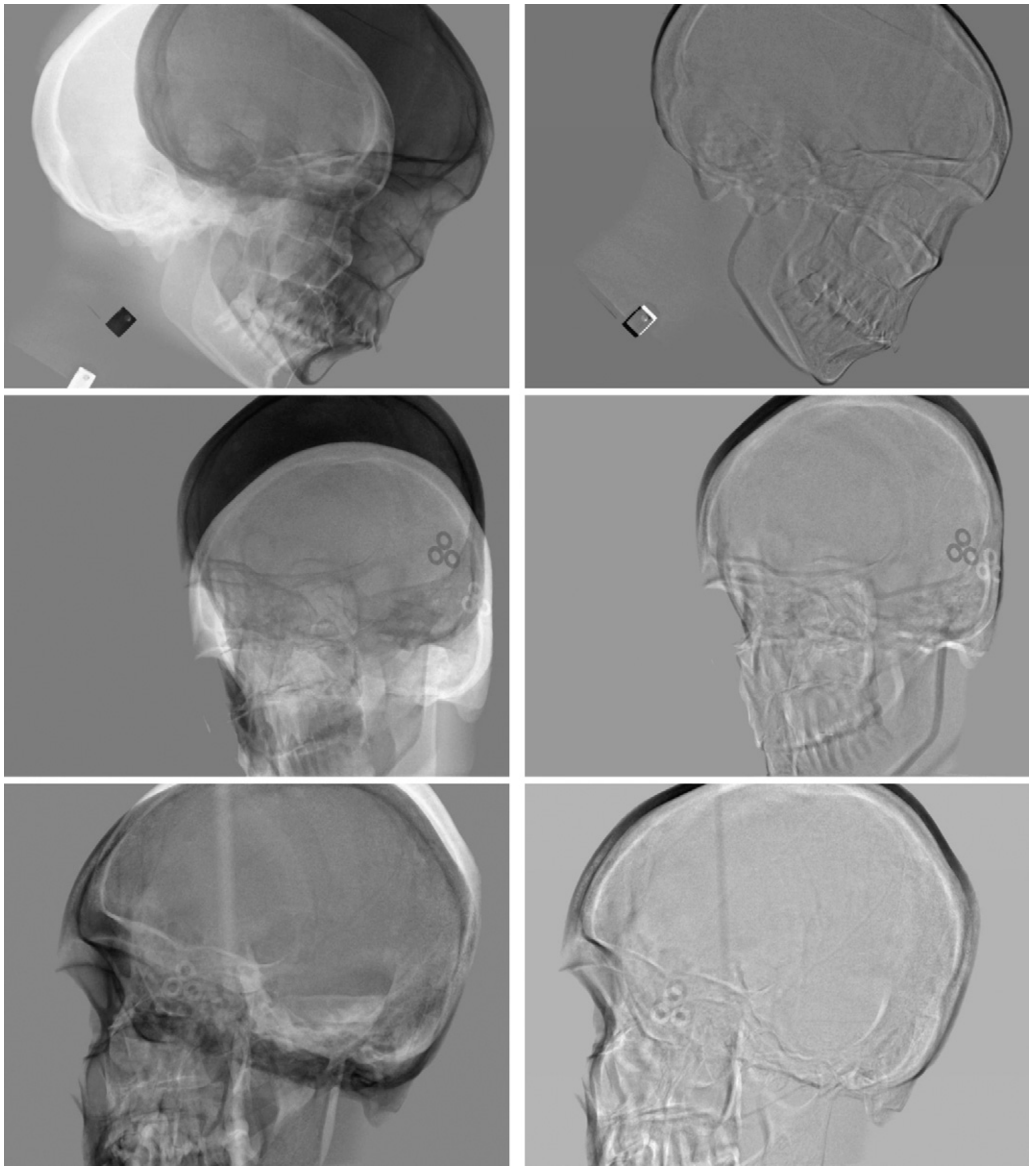

Fig. 9. Registration results of the head phantom. (Left) Subtraction images with motion artifacts and (right) corrected DSA images.

for each of the six dimensions and for both abdominal and head phantoms. An additional fill image (mask) was captured for each scenario half-way of the displacement interval and was considered the true registration position. The six similarity measures (SSD, SAVD, RUI, NCC, VOD and EHD) were computed as a function of the transformation parameters.

The main evaluation criterion is the distance between the computed global extremum and the ground truth. Fur-

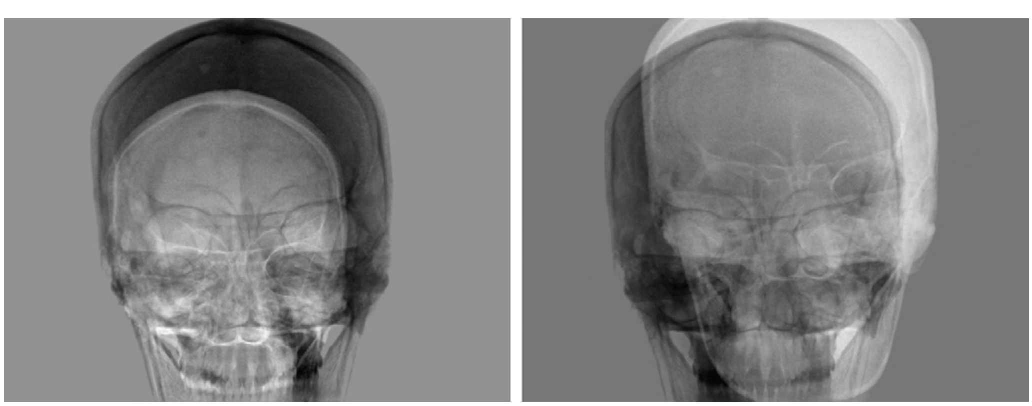

Fig. 10. Registration results of the head phantom. (Left) Subtraction images with motion artifacts and (right) failure in motion compensation due to depth misalignment.

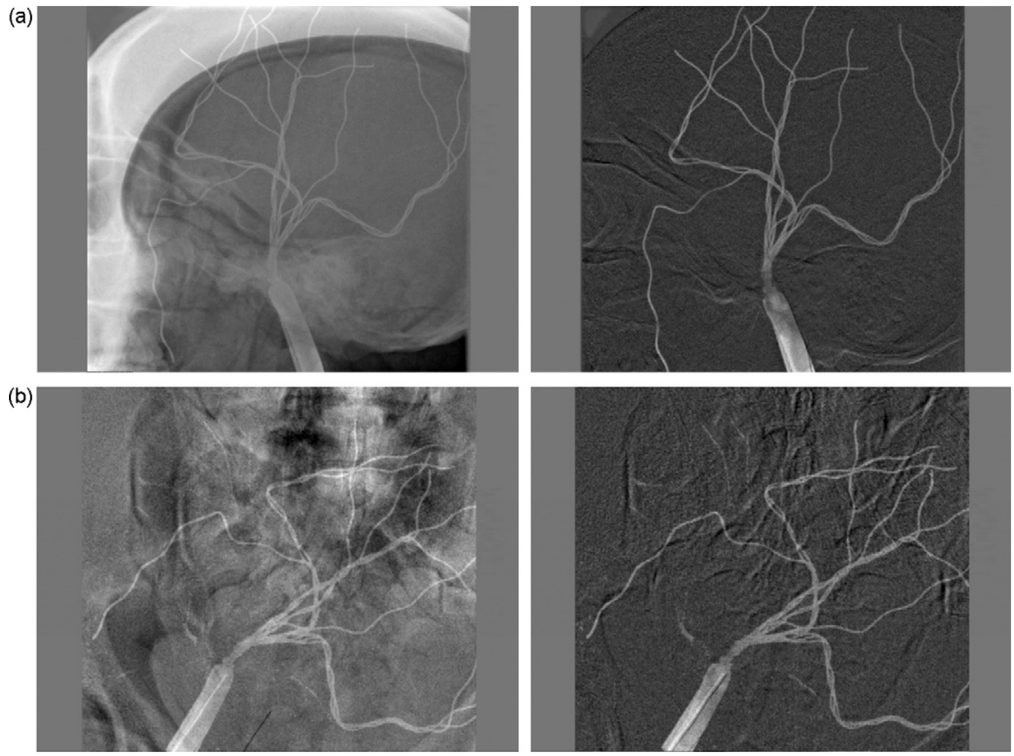

Fig. 11. Registration results of the head and abdomen phantom. (Left) Subtraction images with motion artifacts and (right) corrected RM images.

ther, the smoothness and the number of local extrema is as well crucial for the optimization. A smooth and convergent function without locals is significantly less computational expensive to optimize. Fig. 6 summarizes the mean distance and number of locals, respectively, for each of the measurements.

As expected, all measures performed similarly well for the translational dimensions (see Fig. 7(a) and (b)). Appearance changes in these dimensions are significant and rather caused by structures' arrangement than by superimposition, and therefore accurately inferable though intensity-based measures.

Oppositely, a considerable variations was observed in case of the rotational dimensions (see Fig. 7(c) and (d)). The SSD and the SAVD functions are noisy showing multiple locals for these cases and therefore are not appropriate for our approach. The results for EHD, RIU, NCC and VOD were similar for each evaluation. However, the noise level of the VOD functions is for almost all cases lower compared to that observed for the other functions. Consequently, we conclude that VOD is the most adequate measure to compare fluoroscopic intra-operative images.

Meijering [8] found out that the EHD measure is the most appropriate for DSA diagnostic image registration. Since our evaluation did not illustrate that, we refined our EHD implementation by increasing the histogram of differences resolution. Nonetheless, no significant improvement could be observed. The evaluation of the VOD and EHD using the two dimensional dataset confirmed the superiority of the former for fluoroscopic images (see Fig. 8).

4.2. Registration accuracy

The accuracy of the proposed approach was evaluated by simulating patient motion through displacing the C-arm acquisition system by a random but known value. Starting with this new position our framework computes an optimal position which compensates the induced displacement. The position of the C-arm acquisition system is represented by the vector x_T^*, expressed as $(\alpha, \beta, \gamma, t_x, t_y, t_z)$, where rotation is given in 0.1° and translation in millimeters. The evaluation is performed by comparing the differences between the initial and computed position parameters, as well as the differences between the initial and computed subtraction images.

Fig. 9 shows the results of the registration for the head-phantom, where only native X-ray images were used. The acquisition system was initially positioned to comprehend the whole structure of the phantom, in each case from a different perspective. The left column shows the misaligned images while the right column the corresponding subtractions after motion compensation. It is important to notice that the induced motion is higher then under real clinical conditions. Nevertheless, it can be observed that artifacts are considerably suppressed after registration.

In Fig. 10 the subtraction images before and after registration are disturbed similarly by major motion artifacts. The estimation of the pose component t_z, which is perpendicular to the X-ray detector failed affecting the registration. Depth estimation is difficult, especially if other pose components are misaligned. This effect was observed only for large depth displacements, which are unusual in practice.

Fig. 11 shows results of the registration for the head and abdomen phantom under simulated image-guided intervention circumstances. A cupreous tube model and a fine cupreous wire were used to model the blood vessels and respectively the guide wire. Copper has a higher radio-density than common contrast agents, which implies a higher gray-level differences between live and mask images, and consequently a harder registration problem than in interventions. The left column shows the subtraction images after patient motion occurs, while the right column shows the subtraction images after motion compensation. It can be observed that the artifacts are drastically reduced for both scenarios. As expected, the guide wire is visible through the blood vessels, confirming the accuracy of the approach. The quality of the head-phantom image is considerably better than that for the abdomen-phantom, explained

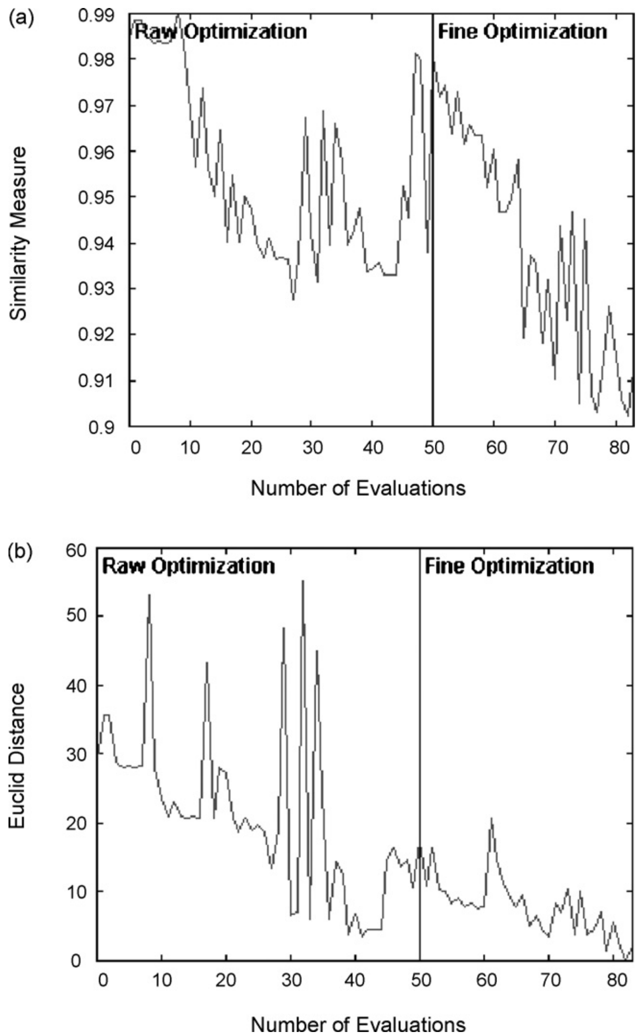

Fig. 12. The similarity measure and the Euclidean distance between known an current optimum as functions of number of evaluations.

by the higher X-ray absorption of the abdominal tissues resulting into a higher quantum noise.

Overall, the mean translation and rotation error, measured in the 3D space was 10.13 mm and 14.59° with a standard deviation of 7.06 and 7.79, respectively. The error in the subtraction images, which is decisive in 2D image registration problems and obtained after the 2D projection during acquisition, is significantly lower according to the results presented above.

Potential artifacts induced by non-rigid motion can be tackled using an independent image-based registration approach applied posterior to our method. These methods are expected to perform significantly more accurate after eliminating the rigid motion through the proposed acquisition-related compensation approach.

The main limitation of the proposed approach is given by the C-arm X-ray acquisition system. Since common C-arms are not designed to perform high precision movements, the positioning precision is limited. C-arm bouncing after positioning further reduces accuracy in some cases.

4.3. Performance analysis

The number of similarity measure evaluations and the number of steps performed during the optimization process are the two characteristic values of the performance analysis. These coincide with the number of repositioning and acquired live images, and are also directly related to the amount of radiation. On average the system requires 118 measure evaluations in order to perform the registration.

Fig. 12 shows the similarity measure and the Euclidean distance between the known and current optimum as functions of number of evaluations. The trend of these functions and their correlation underlines the reliability of the similarity measure as well as the convergence behavior of the optimization approach.

The main drawback of the proposed method is the amount of time required to perform one measure evaluation. Within the current implementation 15 s are needed on average. The time required for acquisition system repositioning, image acquisition and transfer represents over 95% of the total time, only the rest is being used for image processing. Hence, even faster feature-based methods are not expected to significantly reduce computation time.

5. Summary

This paper presents a novel method for motion artifacts compensation in DSA, primarily designed for image-guided interventions. The motion compensation is formulated as a classical pose estimation problem solved by combining acquisition-related solution with image-based registration. Instead of estimating a geometrical transformation, as in common image-based registration approaches, we determine the pose of the acquisition system, for which the disturbing motion artifacts are corrected. Independent usage of image-based registration methods [8,9] is facilitated for the correction of non-rigid motion artifacts and is expected to perform more accurate applied posterior to the rigid motion compensation.

In order to estimate the pose of the acquisition system, an efficient hierarchical optimization algorithm for acquisition-based registration approaches of DSA was developed. This includes a coarse optimization based on a multi-dimensional extension of the golden section search algorithm [17], a simplex estimation refinement [18] and a validation procedure.

The objective function, which relies on variance of differences (VOD), was chosen after performing a novel validation of intensity-based similarity measures for fluoroscopic interventional images.

The approach was evaluated using the AXIOM Artis *d*MP (Siemens Medical Solutions) C-arm X-ray system, and phantoms of anatomical parts made of real human bones. The algorithm yielded robust results for both small and large motion, being more resilient to the fundamental problems of pure image-based registration.

The proposed method is subject to some limitations. For instance, the time costs required to perform one measure evaluation are high due to reposition latency of the C-arm acquisition system. New generation acquisition systems are expected to overcome this limitation. Likewise, image transfer latency can be eliminated by integrating our framework into the standard environment of the imaging system. Future work will include improving the registration accuracy via posterior applied image-based registration methods and clinical validation.

Acknowledgments

This work was supported by Siemens AG Medical Solution AX, Forchheim, Germany. The authors thank the members of Siemens Corporate Research, IDS and Siemens Corporate Technology SE SCR2 for offering comments and suggesting correction.

References

[1] Turski P, Stieghorst M, Strother C, Crummy A, Lieberman P, Mistretta C. Digital subtraction angiography 'road map'. American Journal of Roentgenology 1982;139(6):1233–4.
[2] Oppelt A. Imaging systems for medical diagnostics. Erlangen: Siemens AG, Publicis Corporate Publishing; 2005.

[3] Boxt L. Intravenous digital subtraction angiography of the thoracic and abdominal aorta. Cardiovascular and Interventional Radiology 1983;6(4–6): 205–13.
[4] Foley W, Stewart E, Milbrath J, SanDretto M, Milde M. Digital subtraction angiography of the portal venous system. American Journal of Roentgenology 1983;140(3):497–9.
[5] Guthaner D, Wexler L, Enzmann D, Riederer S, Keyes G, Collins W, et al. Evaluation of peripheral vascular disease using digital subtraction angiography. Radiology 1983;147(2):393–8.
[6] Enzmann D, Freimarck R. Head immobilization for digital subtraction angiography. Radiology 1984;151(3):801.
[7] Kelly W, Gould R, Norman D, Brant-Zawadzki M, Cox L. ECG-synchronized DSA exposure control: improved cervicothoracic image quality. American Journal of Roentgenology 1984;143(4):857–60.
[8] Meijering E. Image enhancement in digital X-ray angiography. Dissertation. University Medical Center Utrecht, Image Sciences Institute; 2000.
[9] Bentoutou Y, Taleb N, Chikr El Mezouar M, Taleb M, Jetto L. An invariant approach for image registration in digital subtraction angiography. Pattern Recognition 2002;35(12):2853–65.
[10] Oung H, Smith A. Real time motion detection in digital subtraction angiography. In: Proceedings of the international symposium on medical images and icons. Silver Spring, USA: IEEE Computer Society Press; 1984. p. 336–9.
[11] Alter T. 3-D pose from 3 points using weak perspective. IEEE Transactions on Pattern Analysis and Machine Intelligence 1994;16(8):802–8.
[12] Schnabel J, Crum B. Image registration and validation. I. Concepts, feature and image registration. Technical report. Computational Imaging Science Group, Division of Imaging Sciencem, Guy's, King's and St. Thomas' Medical School, King's College London; 2004.
[13] Potel M, Gustafson D. Motion correction for digital subtraction angiography. In: Frontiers of engineering and computing in health care: proceedings of the 5th annual international conference of the IEEE engineering in medicine and biology society. 1983. p. 166–9.
[14] Hahn D, Hornegger J, Bautz W, Kuwert T, Roemer W. Unbiased rigid registration using transfer functions. In: Medical imaging: image processing, vol. 5747. San Diego, California, USA: The International Society for Optical Engineering; 2005. p. 151–62.
[15] Cox G, de Jager G. Automatic registration of temporal image pairs for digital subtraction angiography. In: Medical imaging: image processing, vol. 2167. Bellingham, Washington, USA: The International Society for Optical Engineering; 1994. p. 188–99.
[16] Buzug T, Weese J, Fassnacht C, Lorenz C. Using an entropy similarity measure to enhance the quality of DSA images with an algorithm based on template matching. In: Proceedings of the visualization in biomedical computing (VBC'97), vol. 1131. London, UK: Springer-Verlag; 1996. p. 235–40.
[17] Press W, Teukolsky S, Vetterling W, Flannery B. Numerical recipes in C++: the art of scientific computing. Cambridge, USA: Cambridge University Press; 2002.
[18] Nedler J, Mead R. A simplex method for function minimization. The Computer Journal 1965;7:308–13.

Razvan Ionasec was born in Timisoara, Romania, in 1982. He is studying Computer Science at the University of Erlangen-Nuernberg, Germany. Since 2002, he has been working with Siemens Corporate Technology, Germany and US, where he is research assistant in computer vision. His research interests focus on medical imaging and machine learning.

Benno Heigl was born in Regensburg, Germany in 1972. He received the Diploma degree from the University of Erlangen-Nuremberg in 1997 and the PhD in 2003 in the field of image-based modeling, combining approaches from computer vision and computer graphics. Since 2001, he has been with Siemens AG Medical Solutions, Angiography, Fluoroscopic- and Radiographic Systems in Forchheim, Germany. There he is heading a team being responsible for the product development of C-arm CT (DynaCT) and image fusion applications.

Joachim Hornegger graduated in Theoretical Computer Science/Mathematics (1992) and received his Ph.D. degree in Applied Computer Science (1996) at the University of Erlangen-Nuremberg (Germany). His PhD thesis was on statistical learning, recognition, and pose estimation of 3D objects. Joachim was an assistant professor at the University of Erlangen-Nuremberg (1996/1997), a visiting scientist at the Technion (Haifa, Israel), a visiting scholar at the Massachusetts Institute of Technology (Cambridge, MA, USA), and a visiting scholar and lecturer at Stanford University (Stanford, CA, USA) in the academic year 1997/1998. In 1998 he joined Siemens Medical Solutions Inc., where he was working on 3D angiography. In November 2001 Joachim was promoted to director of medical image processing, and in March 2003 director of imaging systems. In parallel to his responsibilities in industry he was a lecturer at the Universities of Erlangen (1998–1999), Eichstaett-Ingolstadt (2000), and Mannheim (2000–2003). Joachim is the author and coauthor of more than 150 scientific publications including a monography on applied pattern recognition and a book on statistical object recognition. Besides his education in computer science, in 2003 Joachim also achieved a diploma in Advanced Management (Cross Functional and General Management, Entrepreneurship, Accounting and Controlling) from the Fuqua School of Business (Duke University, NC, USA) and Siemens. In October 2003 Joachim became professor of Medical Image Processing at the University of Erlangen-Nuremberg, and since October 2005 he is a chaired professor heading the Institute of Pattern Recognition. His main research topics are currently medical image processing, medical vision, and discrete tomography. He is a member of IEEE Computer Society and GI.